Modeling actual water use under different irrigation regimes at district scale: Application to the FAO-56 dual crop coefficient method

Luis-Enrique Olivera-Guerra, Pierre Laluet, Víctor Altés, Chloé Ollivier, Yann Pageot, Giovanni Paolini, Eric Chavanon, Vincent Rivalland, Gilles Boulet, Josep-Maria Villar, et al.

Agricultural Water Management 278 (2023) 108119

Contents lists available at ScienceDirect

Agricultural Water Management

journal homepage: www.elsevier.com/locate/agwat

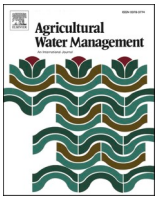

Modeling actual water use under different irrigation regimes at district scale: Application to the FAO-56 dual crop coefficient method

Luis-Enrique Olivera-Guerra [a,*], Pierre Laluet [a], Víctor Altés [b], Chloé Ollivier [a], Yann Pageot [a], Giovanni Paolini [c], Eric Chavanon [a], Vincent Rivalland [a], Gilles Boulet [a], Josep-Maria Villar [b], Olivier Merlin [a]

[a] Centre d'Etudes Spatiales de la Biosphère (CESBIO), Université de Toulouse, CNES, CNRS, IRD, UPS, Toulouse, France
[b] Department of Environmental and Soil Sciences, University of Lleida, Spain
[c] isardSAT, Marie Curie 8-14, Parc Tecnològic Barcelona Activa, Barcelona, Spain

ARTICLE INFO

Handling Editor - B.E. Clothier

Keywords:
Irrigation module
Irrigation amounts
Data assimilation
Water balance model

ABSTRACT

The modeling of irrigation in land surface models are generally based on two soil moisture parameters $SM_{threshold}$ and SM_{target} at which irrigation automatically starts and stops, respectively. Typically, both parameters are usually set to optimal values allowing to fill the soil water reservoir with just the estimated right amount and to avoid crop water excess at all times. The point is that agricultural practices greatly vary according to many factors (climatological, crop, soil, technical, human, etc.). To fill the gap, we propose a new calibration method of $SM_{threshold}$ and SM_{target} to represent the irrigation water use in any (optimal, deficit or even over) irrigation regime. The approach is tested using the dual-crop coefficient FAO-56 model implemented at the field scale over an 8100 ha irrigation district in northeastern Spain where the irrigation water use is precisely monitored at the district scale. Both irrigation parameters are first retrieved at monthly scale from the irrigation observations of year 2019. The irrigation simulated by the FAO-56 model is then evaluated against observations at district and weekly scale over 5 years (2017–2021) separately. The performance of the newly calibrated irrigation module is also assessed by comparing it against three other modules with varying configurations including default estimates for $SM_{threshold}$ and SM_{target}. The proposed irrigation module obtains systematically the best performance for each of the 5 years with an overall correlation coefficient of 0.95 ± 0.02 and root-mean square error of 0.27 ± 0.07 hm^3/week (0.64 ± 0.17 mm/day). Unlike the three irrigation modules used as benchmark, the new irrigation module is able to reproduce the farmers' practices throughout the year, and especially, to simulate the actual water use in the deficit and excess irrigation regimes occurring in the study area in spring and summer, respectively.

1. Introduction

Irrigation water use represents more than 70% of the mobilized freshwater at global scale (Foley et al., 2011; Scanlon et al., 2012) and the demand for irrigation water is still rising (Puy et al., 2021; Wada et al., 2013, 2011). Despite the important pressure of agriculture on water resources, information on the amount of irrigated water is often unavailable. Therefore, monitoring and quantifying irrigation over large areas is critical for an efficient management and allocation of water resources, as well as to understand the biogeophysical impacts of irrigation on water cycle and climate (Haddeland et al., 2006; Krakauer et al., 2020; Puma and Cook, 2010; Thiery et al., 2020, 2017).

Even though significant efforts have been made to develop irrigation retrieval methods, the dynamics of irrigation practices is hard to monitor due to the unavailability of consistent irrigation data and the reluctance of farmers and managers to share such data (Foster et al., 2020; Massari et al., 2021). Moreover, irrigation practices are greatly heterogeneous because of the diversity of water needs (mainly driven by crop types, climate and soil conditions), water availability and local agreements, various irrigation systems (e.g., flood, sprinkler and drip) that often coexist within the same irrigated district and farmers' conceptions of irrigation (Massari et al., 2021). In fact, the spatial heterogeneity of irrigation practices and their inter- and intra-annual variabilities, make the representation of the irrigation water use at all

* Corresponding author.
E-mail address: luis.enrique.olivera@gmail.com (L.-E. Olivera-Guerra).

https://doi.org/10.1016/j.agwat.2022.108119
Received 30 August 2022; Received in revised form 11 December 2022; Accepted 14 December 2022
Available online 9 January 2023

scales challenging.

In recent decades, important efforts have been made to model irrigation processes, especially within large-scale land surface (e.g., Haddeland et al., 2006; Ozdogan et al., 2010; Pokhrel et al., 2012; Lawrence et al., 2019) and hydrological (e.g., Hanasaki et al., 2008, 2018; Wada et al., 2014; Jägermeyr et al., 2015) models. Assessing the irrigation effects on climate and associated feedbacks on land water cycle from regional to global scales has received a particular interest (Pokhrel et al., 2016). Some authors have evaluated the impact of irrigation on the partitioning of energy between sensible and latent heat fluxes (de Rosnay et al., 2003; Haddeland et al., 2006; Leng et al., 2013) and its associated cooling effect (Thiery et al., 2020, 2017), on the depletion of groundwater recharge (Leng et al., 2014; Scanlon et al., 2006), on the decrease in streamflow (Haddeland et al., 2006; Tang et al., 2007), and on changes in precipitation patterns (Guimberteau et al., 2012; Puma and Cook, 2010). In general, all the above authors highlighted the crucial need to realistically account for irrigation in future climatic and hydrological projections (Leng et al., 2015; Thiery et al., 2017; Wada et al., 2013).

At the crop field scale, the most widely used approach relies on the formalism of the FAO-56 method (Allen et al., 1998). In this case, irrigations are simulated according to the simulated crop water requirements, similarly to most irrigation schemes in large-scale land surface models. Allen et al. (1998) suggested that an optimal irrigation is applied before or at the moment when the readily available soil water (RAW) is depleted with a water amount smaller than or equal to the root zone depletion to fulfill the soil water storage capacity. RAW is the amount of water that a crop can extract from the root zone without suffering from water stress. It is hence estimated as the difference between the soil moisture at field capacity (SM_{FC}) and the critical soil moisture at the onset of crop water stress ($SM_{critical}$). In practice, FAO-56 model automatically simulates irrigation when the simulated root zone soil moisture reaches $SM_{critical}$ with the amount of water needed to make the simulated soil moisture reach SM_{FC}.

The current irrigation modules of large-scale land surface models follow the same strategy to simulate irrigation according to the simulated crop water requirement, where $SM_{threshold}$ is set to $SM_{critical}$ and the target soil moisture (SM_{target}) to SM_{FC} (e.g., Haddeland et al., 2006). For instance, Ozdogan et al. (2010) implemented an irrigation scheme in the Noah land surface model (Chen et al., 1996). Irrigation is triggered when the soil moisture availability falls below a user-defined $SM_{threshold}$ set to 50% of SM_{FC}, which is defined according to discussions with local experts in Nebraska and California in the United States, followed by trial and error. In Ozdogan et al. (2010), the irrigation water is supplied as precipitation to mimic sprinkler systems, consistent with the technique used in the studied regions (i.e., Nebraska and California). However, the same irrigation module is also used in other regions where irrigation practices are different. For example, Modanesi et al. (2022) recently implemented this module in Germany and Italy, with $SM_{threshold}$ empirically set to 45% in Italy to avoid large overestimations in irrigation amounts using the default threshold value of 50%. The latter calibration strategy (i.e. *by setting $SM_{threshold}$ to a prescribed value as in* Ozdogan et al., 2010) was evaluated by comparing the ~1 km resolution simulations with the observations available in several small (0.4 ha) fields and two (290 and 760 ha) irrigation districts.

Another example is given by the Community Land Model (CLM; Oleson et al., 2013), which also includes an irrigation scheme based on Ozdogan et al. (2010). In CLM, SM_{target} is set to a weighted sum of $SM_{critical}$ and the soil moisture at saturation. The weighting parameter (F_{irrig}) was determined empirically (as 0.7) to approximately match the global irrigation water use estimated in year 2000, according to Shiklomanov (2000). Note that the most recent version of CLM (CLM5; Lawrence et al., 2019) updated the irrigation triggering by improving the representation of $SM_{critical}$ with an explicit water transport through the vegetation and a more physical root water uptake. However, the principle in this module remains identical to the classical approach based on a target soil moisture level as in Ozdogan et al. (2010). Another recent irrigation module proposed in the ISBA land surface model (Druel et al., 2022) adopts a predefined irrigation triggering (based on the soil moisture index) and a fixed water amount per irrigation event. This strategy implies an a priori knowledge of the irrigation practices over the area.

Leng et al., (2013, 2014) suggested that calibrating the irrigation module at global scale may not be suitable for regional studies due to unreasonable simulations compared against census data. Therefore, they calibrated F_{irrig} at the level of administrative units (counties and water resource regions) in the United States by comparing simulated annual irrigation amounts against census data of the year 2000. These studies found a very large spatial variability in F_{irrig} ranging between 0.2 and 1. Leng et al. (2014) also proved that a calibration at a finer scale (counties versus water resource regions) is more suitable for studying highly localized phenomena such as groundwater pumping. Leng et al. (2015) extended this approach to the entire world by calibrating F_{irrig} at national and sub-national scales against the global inventory developed by Siebert et al. (2010). However, the reference data from this global inventory were estimated based on the optimal demand for crop growth, which is probably not a realistic scenario given the variety of irrigation practices and the fact that it is rather difficult for farmers to follow the exact crop water requirement.

In the same vein, Puy et al. (2021) compared the annual irrigation estimates provided at country scale worldwide by eight different global models and showed large discrepancies. Using uniform $SM_{threshold}$ and SM_{target} parameters actually means that these schemes largely ignore the spatial variability and temporal dynamics of irrigation practices. Moreover, irrigation estimates are usually validated against annual data from census and surveys at administrative to country scales (e.g. AQUASTAT, 2016), which are generally unreliable due to bureaucratic and political constraints (Puy et al., 2021). Therefore, most of existing irrigation modules have been calibrated using biased reference data, and have not been validated against actual irrigation water use at temporal scales finer than annual.

In an attempt to address the diversity of irrigation practices and the lack of reliable census data, Felfelani et al. (2018) constrained the spatio-temporal variability of SM_{target} by assimilating in CLM a satellite surface soil moisture product (SMAP). This approach provided promising improvements in irrigation simulations at large scale. However, there are still some shortcomings to overcome, such as i) the spatial resolution of satellite soil moisture products (36 km for SMAP) is not suitable for monitoring the crop water status at the scale of agricultural practices, and ii) discrepancies between the top soil moisture detected by remote sensing and that of the root zone, which is where $SM_{threshold}$ and SM_{target} apply to trigger a simulated irrigation event and refill the root zone soil water reservoir.

Although land surface models have become increasingly accurate in the representation of biophysical processes, they remain still limited with respect to represent the human-related processes like irrigation. In this vein, the above literature review thus clearly highlights the lack of calibration and validation studies of irrigation modules at the spatial and temporal scales of the management of irrigation water and using reliable irrigation observations. To fill the gap, the objective of this study is to evaluate different irrigation modules at the weekly scale over an irrigation district where the water withdrawal is precisely measured. To accomplish this, we develop and test a new calibration method of $SM_{threshold}$ and SM_{target} parameters. We rely on the FAO-56 formalism to model the crop water budget at the field scale as it is widely used by the agricultural community. However, the tested irrigation modules could be easily implemented in more physically-based land surface models.

The study focuses on an irrigation district in northeastern Spain (Algerri-Balaguer) covered by 8100 ha of crops – mainly maize, barley, wheat and fruit trees – irrigated by sprinkler and drip systems. The study area has the particularity of accounting with real-time measurements of irrigation water use at the district scale. The availability of these data is

of great interest to assess the performance of irrigation modules at the scale of the agricultural water management, as well as to quantify the actual water use efficiency to ensure a better management. The main originality of our work is to demonstrate the capability of the irrigation modeling and calibration strategy to retrieve the overall irrigation regime (through the retrieval of $SM_{threshold}$ and SM_{target}) at the spatially integrated district scale.

2. Study area and data

The present study was performed for the period from April 2017 to December 2021 over the Algerri-Balaguer irrigation district (Section 2.1) in northeastern Spain (Catalonia). The data used are composed of the time series of observed irrigation water withdrawals for the district, and the input data to the dual crop coefficient FAO-56 model are: a vegetation index derived from Sentinel-2 satellite data on clear sky days acquired over Algerri-Balaguer, a land cover map, information on soil texture from the global map database SoilGrids (Poggio et al., 2021) and times series of meteorological data collected by two stations included in the study area. A detailed description of the dataset is presented below.

2.1. Algerri-Balaguer district

The Algerri-Balaguer irrigation district is located north of Lleida in the Ebro basin. Lleida has a semi-arid continental Mediterranean climate typical of the Ebro valley, with a mean annual air temperature, rainfall and number of rain days of 16 °C, 340 mm and 60, respectively. The irrigation district covers about 8100 ha of cropped lands, the main crop types (~85%) being maize, barley, wheat, fruit trees and alfalfa. More than 50% of the district is cultivated by double crops with winter cereals (mainly barley) and maize in summer. Irrigation is applied over about 75% of the area either using sprinkler (systematically for annual crops) or drip (systematically for fruit trees) systems. The rest (25%) is a rainfed dryland area covered by winter cereals (barley). An overview of Algerri-Balaguer district is presented in Fig. 1.

2.2. Irrigation data

The Algerri-Balaguer district is fed with the Pyrenees water, which is transported and stored by an extensive irrigation network built within the Ebro basin (Milano et al., 2013). The water is pumped in the Noguera Ribagorçana River and transported by gravity through the irrigation canals of Algerri-Balaguer to be stored in upstream reservoirs and then used for irrigation in the downstream crops. The pumped water is measured in real time by the Automatic Hydrological Information System (SAIH) of the Ebro basin. The pumped water data are aggregated at weekly scale (shown in Fig. 2) in order to dampen the potential time lag of several days between the water pumping and actual application of irrigation water at field level. In this study, the irrigation water use observations are derived from the pumped water volume reduced by 5.8%, considering losses by evaporation and leaks during the transfer from the river and reservoir to the fields. The losses were estimated for the year 2021 from the annual water withdrawn from the river and the data provided by water counters distributed in the district and sporadically collected by the Algerri-Balaguer district agency. This estimation was only available for the year 2021.

2.3. Sentinel-2 NDVI

Sentinel-2 (S2) is a wide-swath, high-resolution, multispectral imaging mission with a global 5-day revisit frequency, consisting of two satellites: Sentinel-2A and Sentinel-2B launched in June 2015 and March 2017, respectively, and managed by the European Space Agency (ESA). The study period from April 2017 to December 2021 is defined to ensure the availability of satellite images throughout the entire period with similar frequency. The Multispectral Instrument (MSI) on-board both S2 platforms samples 13 spectral bands, from which only the red (band 4) and near-infrared (band 8) data at 10-m spatial resolution are used in this study to estimate the normalized difference vegetation index (NDVI). The S2-derived NDVI is used to monitor the state and phenology of crops. We used the Level-2A orthorectified atmospherically corrected surface reflectances. First, the cloud mask band (QA60) is applied in order to remove pixels contaminated by opaque clouds. A second cloud masking is applied from the cirrus band (band 10). If more than 25% of pixels inside a given field were removed by the cloud masking procedure, then all pixels inside this field were removed in order to avoid cloud contamination. Conversely, if less than 25% of pixels inside a given field were affected by clouds, then, the S2 NDVI data were aggregated at the field scale by averaging the NDVI pixels falling inside the plots delineated by the land cover map of each year from 2017 to 2021, separately. Finally, the field-scale NDVI data are interpolated at the daily scale by using a Piecewise Cubic Hermite Interpolating Polynomial method (Fritsch and Carlson, 1980).

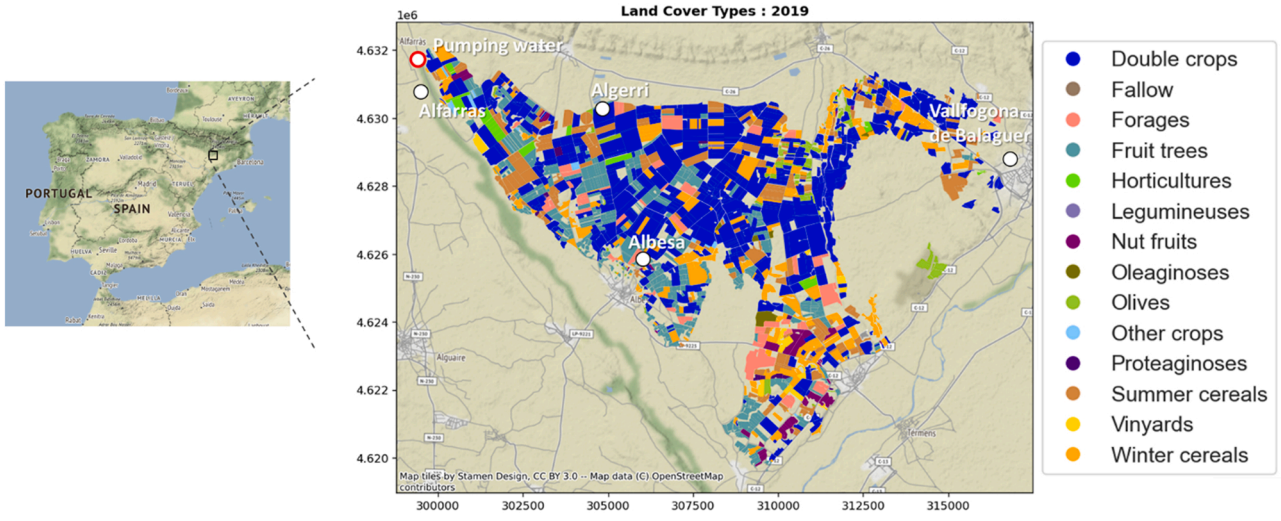

Fig. 1. Map of land cover classes in Algerri-Balaguer irrigation district for the year 2019. It is also indicated the Algerri, Albesa, Alfarras and Vallfogona de Balaguer meteorological stations (black circles) and the pumping station (red circle) where water is withdrawn from the Noguera Ribagorçana River to irrigate the district.

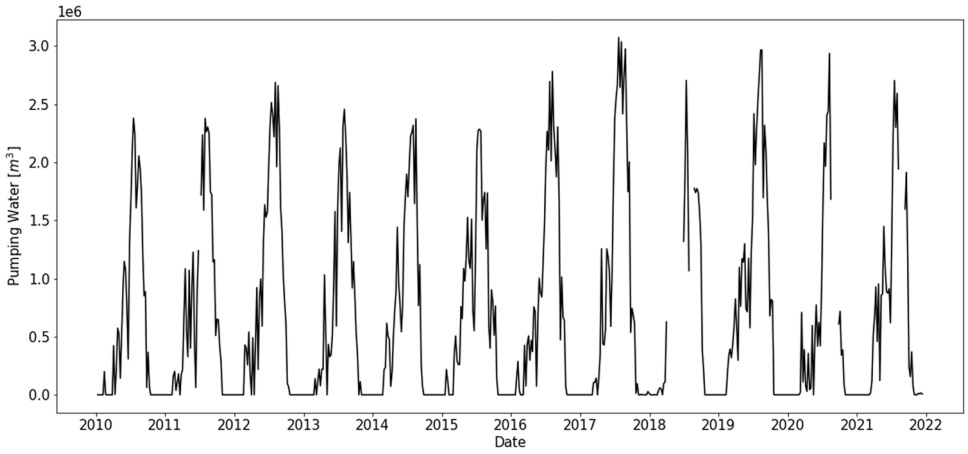

Fig. 2. Time series of the weekly pumped water volume to irrigate the Algerri-Balaguer district for the period 2010–2021.

2.4. Land cover map

A detailed land cover map is obtained from the Geographic Information System for Agricultural Parcels (SIGPAC) and the Single Agricultural Declaration (DUN) document. SIGPAC is a public registry of an administrative nature that contains information on the fields at 1:5000 scale and 25 cm spatial resolution and DUN is a yearly mandatory declaration about the agricultural exploitation that each farmer of an agricultural productive area must provide. Annual SIGPAC and DUN products are extracted from https://analisi.transparenciacatalunya.cat/ . The products provide the crop type of each plot land and whether it is irrigated or not (dryland). Since the SIGPAC database is produced on a yearly basis, there is no information about the presence of double crops although they should be included for estimating the total water use. Therefore, we added to the original SIGPAC database a new class (double crops). Such a classification is based on the detection of a second peak in the annual S2 NDVI time series. Note that the plots smaller than 100 m^2 (after subtracting a buffer of 10 m) are removed to avoid plots whose pixels are all affected by border effects taking into account the 10-m spatial resolution of NDVI data.

2.5. Soil data

Soil properties are obtained from the global ISRIC (International Soil Reference and Information Centre) SoilGrids data set v2.0 updated from its previous version (Hengl et al., 2017; Poggio et al., 2021). SoilGrids has a spatial resolution of 250 m and provides soil texture information that is the clay, sand and silt contents and their uncertainty at different depths. The clay and sand percentages of the 0–5, 5–15, 15–30, 30–60 and 60–100 cm layers are linearly averaged to estimate their effective values over the 1-m deep soil profile. Soil information for deeper layers is not used given that they are more uncertain. The estimated uncertainty in clay and sand percentages is estimated to be less than 3% in the 1-m soil profile over the Algerri-Balaguer district. Finally, the 250-m resolution and 0–1 m deep sand and clay percentages are averaged at the plot scale using the SIGPAC annual maps, as for NDVI data.

2.6. Meteorological data

The meteorological data are obtained from 4 stations (Algerri, Alfarras, Albesa and Vallfogona de Balaguer) located in Algerri-Balaguer district and belonging to the Catalan meteorological network. Data are available at https://ruralcat.gencat.cat/web/guest/agrometeo.estacions. Both stations provide daily air temperature, air humidity, wind speed, solar radiation, reference evapotranspiration and precipitation. There is very little difference between simultaneous measurements at the 4 stations (not shown), so that the meteorological variables are considered to be uniform over the irrigation district and set to the mean of individual measurements.

3. Methodology

Irrigation modules are traditionally constrained to estimate irrigation in an optimal scenario, not being able to estimate actual irrigation in the case of excess or deficit irrigation. In reality, irrigation practices are likely to change along the year according to the crop development and the atmospheric demand (e.g. irrigation more frequent and intense during summer and the opposite in winter), so it is rather difficult for farmers to follow the exact crop water requirement. Therefore, farmers often overestimate and/or underestimate irrigation throughout the agricultural season. To fill this gap in irrigation modules, we propose to invert irrigation parameters ($SM_{threshold}$ and SM_{target}) in time in order to reproduce the dynamics of irrigation practices along the year (detailed in Section 3.3). In this study, we take advantage of the FAO-56 model (Allen et al., 1998) to implement different irrigation modules, including the classical one originally used by the FAO-56 model. The performance of the different irrigation modules is evaluated to estimate the actual irrigation water use at weekly and district scale. The overall approach for testing the irrigation modules is: 1) the FAO-56 model is implemented at the field scale over the entire Algerri-Balaguer area, 2) both irrigation parameters ($SM_{threshold}$ and SM_{target}) are inverted at district/month scale from the assimilation of 2019 irrigation observations into the FAO-56 model, 3) both retrieved parameters are used as input to the FAO-56 model, which is run over 5 separate years (from 2017 to 2020) and, 4) the irrigations simulated at district scale are compared with observations at weekly scale, and the impact of the temporal variability of $SM_{threshold}$ and SM_{target} is assessed. Each step is detailed in the following sections. The overall methodology is summarized in the schematic diagram of Fig. 4.

3.1. FAO-56 dual crop coefficient model

The FAO-56 dual crop coefficient model (FAO-2Kc; Allen et al., 1998) is a water balance model to simulate the crop evapotranspiration (ET). The FAO-2Kc model is driven by 1) meteorological forcing variables to calculate reference evapotranspiration (ET_0) and 2) the water supply from precipitation and irrigation to simulate the soil water availability for soil evaporation and plant transpiration. According to the FAO-2Kc formalism, the daily water balance is expressed as:

$$Dr_t = Dr_{t-1} + ET_t - P_t - I_t + DP_t + CR_t + RO_t \quad (1)$$

where Dr is the root zone depletion, P the precipitation, I the irrigation, DP the deep percolation, CR the capillarity rise and RO the surface

runoff. Every term is expressed in mm for the day *t* (and *t-1* for Dr). The RO and CR term are neglected due to fairly flat surfaces and a water table deeper than 2 m in the study area (the Algerri-Balaguer district is equipped with 2-m deep drains to prevent any rise of the water table). DP is estimated as the rest of the Eq. (1). ET is estimated by multiplying ET_0 by two separate crop coefficients for transpiration and evaporation as follows:

$$ET = (Ks \bullet Kcb + Ke)ET_0 \quad (2)$$

where Kcb is the basal crop transpiration, Ks (0−1) the water stress coefficient that reduces the potential transpiration (T/Kcb•ET_0) and Ke the evaporation coefficient that is also regulated by an evaporation factor Kr. ET_0 is calculated according to the FAO Penman–Monteith equation (Allen et al., 1998) at daily scale and Kcb is estimated from a linear relationship with fraction of vegetation cover (FC) as:.

$$Kcb = FC_t * Kslope_{crop} + Koffset_{crop} \quad (3)$$

with $Kslope_{crop}$ and $Koffset_{crop}$ being two parameters depending on crop type and whose values are obtained from literature and presented in Table 1. FC_t at day t is estimated from daily NDVI as in Eq. (3), but using the parameters $Fslope_{crop}$ and $Foffset_{crop}$ reported in Table 1. Fig. 3 illustrates the time series of mean Kcb in 2021 for the main crop types over Algerri-Balaguer district.

Ks is calculated based on daily computation of the water balance for the root-zone layer Zr (m) as follows:

$$K_s = \frac{TAW - D_r}{TAW - RAW} = \frac{TAW - D_r}{TAW(1-p)} \quad (4)$$

where Dr (mm) is calculated from the daily water balance according to the Eq. (1), TAW (mm) is the total available soil water in the root zone, and p is the fraction of TAW that a crop can extract from the root zone without suffering from water stress determining RAW (p•TAW). According to Allen et al. (1998), p is a crop-specific parameter that controls the water depth threshold below which irrigation should be triggered to avoid crop water stress, by keeping Dr smaller than RAW (Ks = 1). TAW is estimated as the difference between SM_{FC} and the water content at wilting point (SM_{WP}) by the daily crop rooting depth (Zr) as:

$$TAW = 1000(SM_{FC} - SM_{WP})Zr \quad (5)$$

The soil parameters SM_{FC} and SM_{WP} are estimated using the clay and sand contents from SoilGrids data and following the pedotransfer function proposed by Román Dobarco et al. (2019). In Algerri-Balaguer district, SM_{WP} and SM_{FC} are quite homogeneous with values of 0.207 (± 0.006) and 0.330 (± 0.005) m^3m^{-3}, respectively. The rooting depth Zr is assumed to vary between a minimum value Zr_{min} (maintained during the initial crop growth stage and set to 0.1 m for annual crops) and a maximum value Zr_{max} (reached at the maximum NDVI per plot in the agricultural season). Zr is thus expressed as:

$$Zr_t = Zr_{min} + FC_t(Zr_{max} - Zr_{min}) \quad (6)$$

The Kr soil evaporation reduction coefficient is simulated by the surface depletion water in the surface evaporable layer and according to Merlin et al. (2016) to take into account its dependence to soil texture. The texture-based method for Kr has been derived and evaluated over a variety of sites and clay/sand contents (Lehmann et al., 2018; Merlin et al., 2016) and recently implemented into the FAO-2Kc model by Amazirh et al. (2021) as:

$$K_r = \left[0.5 - 0.5\cos\left(\frac{\pi \bullet SSM}{SM_{Saturation}}\right)\right]^P \quad (7)$$

where SSM is the actual surface soil moisture, $SM_{Saturation}$ is the soil moisture at saturation and P is a semi-empirical parameter depending on the depth of soil moisture estimates and soil properties (texture) (Amazirh et al., 2021; Merlin et al., 2016). As SSM is not explicitly estimated in the FAO-2Kc model, it is derived from the surface soil water depletion (De), the total evaporable water (TEW) and the soil evaporation layer depth (Ze in m) as:

$$SSM = 0.5 \bullet SM_{WP} + \frac{TEW - De}{1000 \bullet Ze} \quad (8)$$

3.2. Irrigation module

The FAO-2Kc model can be used to simulate irrigation by assuming that irrigation events occur at the onset of the crop water stress. In practice, the simulated irrigation is automatically triggered on the day when RAW is depleted (i.e., Dr = RAW), and the irrigation dose is estimated as the water amount necessary to fulfill the water storage capacity and to get back up to the field capacity (soil moisture equal to SM_{FC}). Therefore, the FAO-2Kc model classically simulates irrigation events in an optimal scenario along the season, in order to maintain crop under unstressed conditions without generating surplus water.

We can thus define the I-dose parameter as the irrigation water volume (in mm) applied per irrigation event over a given field. An irrigation event is triggered (simulated) for each field when the simulated root zone soil moisture reaches $SM_{threshold}$. The root zone soil moisture is simulated from the modeled soil water budget that includes the plant transpiration, soil evaporation and deep percolation terms, which depend on the root zone water depletion (Eq. 1) controlled mainly by the crop transpiration. Therefore, I-dose (mm) can be represented in a generic form as the difference between the soil moisture at which

Table 1
Main parameters of the FAO-2Kc model per crop type used in this study.

Crop type	Fslope (-)	Foffset (-)	Kcb_{max} (-)	Kslope (-)	Koffset (-)	Ze (m)	Zr_{min} (m)	Zr_{max} (m)	p (-)	fw[1] (-)
Winter cereals	1.180	-0.165	1.10	1.47	-0.17	0.10	0.10	1.00	0.55	1.0
Summer cereals	1.215	-0.185	1.15	1.23	-0.14	0.10	0.10	1.00	0.55	1.0
Double crops	1.198	-0.18	1.13	1.35	-0.16	0.10	0.10	1.00	0.55	1.0
Forages	1.180	-0.160	1.15	1.47	-0.17	0.10	0.10	1.00	0.55	1.0
Fruit trees	1.220	-0.170	1.00	1.35	-0.16	0.10	1.00	1.00	0.50	0.3
Nut fruits	1.220	-0.170	0.90	1.35	-0.16	0.10	1.00	1.00	0.40	0.3
Olives	1.220	-0.170	0.65	1.35	-0.16	0.10	1.00	1.00	0.65	0.3
Vinyards	1.220	-0.170	0.65	1.44	-0.10	0.10	1.00	1.00	0.45	0.3
Horticultures	1.220	-0.160	0.95	1.29	-0.09	0.10	0.10	0.45	0.30	1.0
Legumineuses	1.380	-0.300	1.05	1.47	-0.17	0.10	0.10	1.00	0.60	1.0
Oleaginoses	1.380	-0.300	1.05	1.47	-0.17	0.10	0.10	1.00	0.60	1.0
Proteaginoses	1.180	-0.160	1.10	1.35	-0.16	0.10	0.10	0.80	0.38	1.0
Other crops	1.220	-0.170	0.95	1.35	-0.16	0.10	0.15	1.00	0.70	1.0
Fallow[a]	1.180	-0.160	1.15	1.47	-0.17	0.10	0.15	1.00	0.55	1.0

[1] fw is fraction of the soil surface wetted by irrigation.
[a] Fallow is not irrigated.

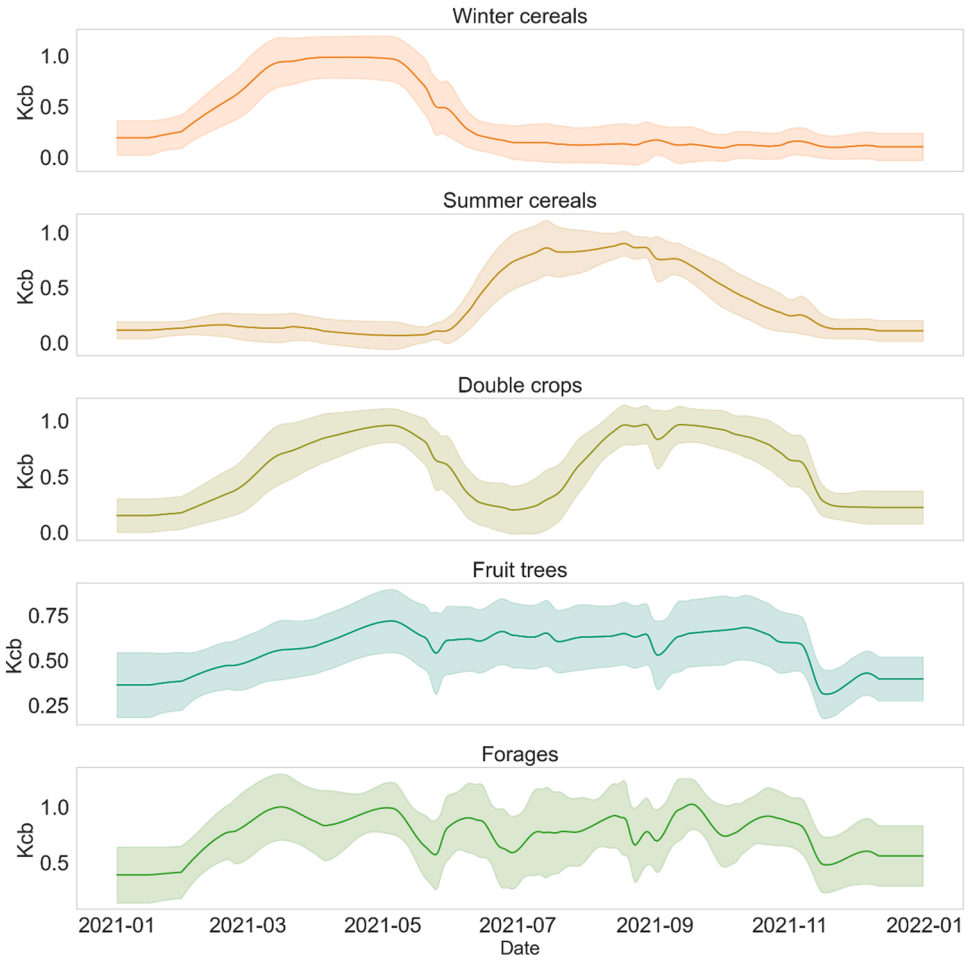

Fig. 3. Time series of the mean (line) and standard deviation (shaded area) of field-scale Kcb values in 2021 for the five main crop types over the Algerri-Balaguer district, separately.

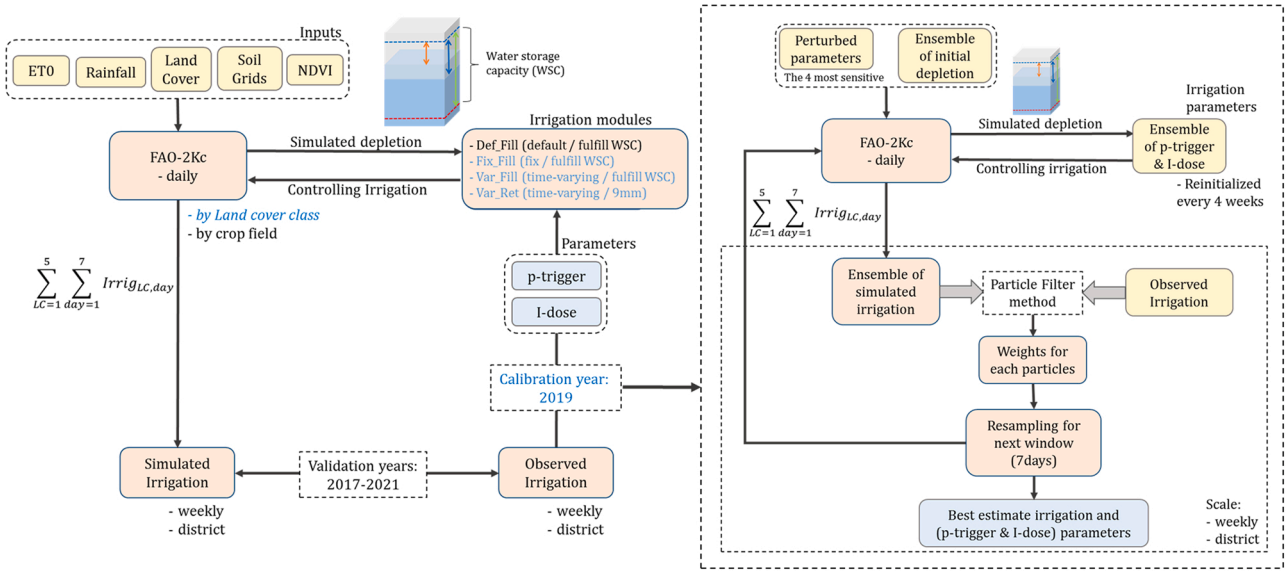

Fig. 4. Schematic diagrams giving an overview of the methodology. On the left is presented the overall calibration/validation approach to test four different irrigation modules by running the FAO-2Kc over 5 years separately. On the right is presented the approach to retrieve the irrigation parameters from the assimilation of irrigation observations during 2019 using a particle filter method.

irrigation automatically starts ($SM_{threshold}$) and stops (SM_{target}) as:

$$Idose = 1000\left(SM_{target} - SM_{threshold}\right)Zr \quad (9)$$

In the case of FAO-2Kc model, $SM_{threshold}$ is usually set to the critical soil moisture at the onset of crop water stress ($SM_{critical}$), while SM_{target} is usually set to the soil moisture at field capacity (SM_{FC}). However, in reality $SM_{threshold}$ and SM_{target} can differ significantly from $SM_{critical}$ and SM_{FC}, respectively. This notably occurs in deficit ($SM_{threshold} < SM_{critical}$) and excess ($SM_{target} > SM_{FC}$) irrigation case, respectively.

Note that in the FAO-2Kc model, $SM_{critical}$ is related to the fraction p (RAW/TAW, threshold below which crop is under water stress). Based on this expression, we can express a threshold for triggering irrigation in a generic form (herein p-trigger) as the ratio between Dr and TAW (unitless), which means the fraction of water depleted in relation to the water storage capacity. Therefore, p-trigger can be related to the $SM_{threshold}$ used by several irrigation schemes (see Section 1) as the complement of the normalized $SM_{threshold}$:

$$ptrigger = 1 - \frac{SM_{threshold} - SM_{WP}}{SM_{FC} - SM_{WP}} \quad (10)$$

Therefore, we can distinguish two key parameters controlling irrigation: the threshold for triggering irrigation (p-trigger) and the irrigation dose applied by irrigation event (I-dose). Note that both parameters allow representing not only an optimal irrigation regime satisfying the crops requirement, but also under-irrigation regimes (implying crop water stress) with a p-trigger lower than the value defined in Allen et al. (1998), and over-irrigation regimes (implying deep percolation) with an I-dose resulting in a root zone soil moisture value exceeding the SM_{FC}. Both irrigation parameters are used in this study to define and test four different irrigation modules, which are summarized in Table 2 and described below.

3.2.1. Avoiding stress and fulfilling the water storage capacity (Classical FAO-2Kc or Def_Fill irrigation module)

The p-trigger in the FAO-2Kc model by default is the crop-tolerance to stress parameter (fraction p) proposed by Allen et al. (1998). It is about 0.4–0.6 for most of crops (crop-specific) and corrected by meteorological conditions. The I-dose is estimated as the water depth to fulfill the water storage capacity (~RAW) making the Dr equal to 0. Therefore, this approach does not allow producing water excess as it simulates the optimal amount of water when it is necessary. Note that after a significant rainfall event no irrigation is needed to supply the crop water needs.

3.2.2. No a priori assumption on p-trigger and irrigation dose (Var_Ret irrigation module)

Both irrigation parameters p-trigger and I-dose are retrieved at the monthly time scale from irrigation observations at the district scale. Such a strategy is expected to provide robust estimates under all (optimal, deficit and over) irrigation regimes.

Table 2
Main characteristics of the four irrigation modules tested in the FAO-2Kc model in terms of the irrigation triggering (p-trigger) and the water amount per irrigation amount (I-dose).

Module name	p-trigger	I-dose
Def_Fill	Fixed to the default (crop specific) value in the FAO-56 to avoid stress	Water amount needed for filling the root-zone soil reservoir
Var_Ret	Time-varying (monthly retrieved) value	Water amount retrieved from the inversion process
Var_Fill	Time-varying (monthly retrieved) value	Water amount needed for filling the root-zone soil reservoir
Fix_Fill	Fixed to the value (0.10) retrieved during summer	Water amount needed for filling the root-zone soil reservoir

3.2.3. No a priori assumption on p-trigger and fulfilling the water storage capacity (Var_Fill irrigation module)

Similarly to Var_Ret, this irrigation module used as input the p-trigger retrieved at monthly scale from observations. However, I-dose is estimated by fulfilling the water storage capacity as in the classical FAO-56 irrigation module. This strategy is adopted in order to evaluate whether fulfilling the water storage reservoir would be adequate to reproduce irrigation for all the year.

3.2.4. p-trigger set to its summer value and fulfilling the water storage capacity (Fix_Fill irrigation module)

Irrigation is triggered by setting the p-trigger to its value retrieved during summer (July-August-September), when irrigation water use is the most intense. The I-dose is estimated by fulfilling the water storage capacity as in the classical FAO-56 irrigation module. This strategy is adopted in order to evaluate whether a p-trigger representative of the most intense irrigation period would be adequate to reproduce irrigation for all the year.

3.3. Inverting irrigation parameters

In this study, both irrigation parameters (p-trigger and I-dose) are inverted from observed irrigations over Algerri-Balaguer district. The retrieval method is based on a particle filter (PF) assimilation approach to estimate jointly irrigations and the parameters controlling irrigation throughout the year. For this purpose, observed irrigations cumulated over a weekly basis are assimilated into the FAO-2Kc model by land cover classes. Both aspects of the retrieval method are detailed below.

3.3.1. Particle filter assimilation method

The PF approach (Vrugt et al., 2013) is used to retrieve p-trigger and I-dose on a weekly basis by assimilating into the FAO-2Kc the observed irrigations over Algerri-Balaguer district. The model state consists of water depletions simulated for both surface and root-zone layers from daily water balance at the end of the assimilation period (7 days). The PF-based assimilation requires an accurate statistical representation of observation and model errors. In this study, random uncertainties in irrigation observations are represented by a standard deviation equal to 10% of their absolute values. Moreover, since irrigation during winter in Algerri-Balaguer district is usually zero, the minimum observation error is set to 0.1 hm^3 (equivalent to a mean water depth over the district of about 0.24 mm/day) to avoid degeneracy and sample impoverishment problems typical of noise-free dynamical systems (Gordon et al., 1993; Moradkhani et al., 2005). In order to represent the modelling uncertainty, the most sensitive parameters of FAO-2Kc model are perturbed according to a normal distribution with a varying standard deviation equal to 10% of their corresponding values. Based on the comprehensive sensitivity analysis of the FAO-2Kc model by Laluet et al. (2022), four main parameters are selected: the maximum rooting depth (Zr_{max}), slope and offset of the linear relationship between Kcb and NDVI as well as the maximum possible Kcb (Kcb_{max}). In addition, the surface and root-zone depletions, including initial states, are perturbed by 10% of their values without considering spatial or temporal autocorrelation.

Initial values of surface and root-zone depletions on the first day of the simulation period (set to the 1st January of a given year) are sampled from a uniform distribution between 0% and 40% of TAW by assuming that the depleted water never exceeds 40% of TAW in winter. This is supported by spin-up FAO-2Kc simulations, which show that for each of the 5 studied years (2017–2021) the depletions simulated at the end of the year are systematically below 40%, even if no irrigation is simulated in November and December.

The parameters to be estimated (p-trigger and I-dose) are also sampled from a uniform distribution with a sampling size set to 300 particles considering all the possible values over the irrigation district.

Specifically, p-trigger is bounded between 0.01 and 0.90 meaning that irrigation is triggered when the root-zone depletion reaches 1% and 90% of TAW, respectively. Similarly, I-dose is bounded between 0 (no irrigation) and 20 mm, which is the maximum range of irrigation amount per event that can be found in the district according to the irrigation systems (drip or sprinkler).

As irrigation practices are likely to change along the year, both irrigation parameters are reinitialized to the initial uniform distribution every 4 weeks. In that case, the irrigation parameters are time-varying and inverted for a window of 4 weeks. The duration (4 weeks) of the assimilation period is a compromise between the temporal dynamics of the parameters (which may change during the agricultural season) and the number of available observations (a time series of four weekly observations in our case). Note that this strategy helps to minimize the degeneracy problem that is more pronounced with longer periods Abolafia-Rosenzweig et al. (2019). To fully avoid degeneracy, the particles are resampled when the so-called effective sample size (Neff) has decreased below the predefined threshold of one third of the initial particle size number (Moradkhani et al., 2005; van Leeuwen et al., 2019).

The assimilation approach is performed 4 times by considering a moving-window starting on January 1, 8, 15 and 22, respectively. Since the 1-month assimilation periods overlap between the four assimilation runs, the parameters estimated from the four runs are averaged on a weekly basis. This is done in order to smooth out the parameter dynamics at the validation (weekly) scale.

3.3.2. Implementation of FAO-2Kc by crop type

In order to minimize the computational cost of running FAO-2Kc hundreds of times (i.e. number of particles size) on each of the ~3000 crop fields in Algerri-Balaguer using a PF, the inversion process is carried out by implementing FAO-2Kc over the five main crop types only. Those five land cover classes are: double cropping (mainly barley followed by maize), winter cereals (mainly barley), summer cereals (mainly maize), fruit trees (mainly peaches, nectarines, pears and apples) and forages (mainly alfalfa).

By simulating irrigation over the ~3000 crop fields from the classical approach, the five main land cover classes account for 94% of the total simulated irrigation over the district (Fig. 5). FAO-2Kc is therefore implemented by land cover class by considering that the area covered by each class is relatively uniform in terms of soil properties (this is verified by SoidGrids data and the small standard deviation in SM_{WP} and SM_{FC} less than 0.006 m^3m^{-3}) and vegetation state. For that, FAO-2Kc inputs like NDVI and soil properties are first averaged by land cover class in order to build a dataset by land cover type. The model is then run to simulate the irrigation depths (mm) for each of the five classes separately, and the irrigation simulated per class is finally aggregated at the district scale by considering their respective areas within Algerri-Balaguer district. The remaining 6% of irrigation water consumed by the rest of land cover classes is represented by the average behavior in water consumption of the main five classes.

3.4. Calibration/validation strategy

The calibration process is carried out by implementing the FAO-2Kc model as described above for 2019 and illustrated in Fig. 4, since it is the only year without missing data in both observed irrigations and S2-NDVI.

Once the time-varying parameters are calibrated in 2019, they are used to implement the four irrigation modules (Def_Fill, Fix_Fill, Var_Fill and Var_Ret) for each of the 5 years between 2017 and 2021, separately. Unlike the calibration process where FAO-2Kc is implemented at land cover level over the five main crop types, the FAO-2Kc model is run over all the ~3000 crop fields for validation and intercomparison purposes, including all land cover classes. The irrigation estimates from the four irrigation modules are evaluated against observations in order to assess how the parameters p-trigger and I-dose impact the performance of FAO-2Kc to reproduce at the irrigation district scale the actual irrigation practices along the season.

4. Results and discussion

4.1. Retrieving irrigation parameters

The model parameters representing farmers' irrigation practices over the Algerri-Balaguer district are retrieved for the year 2019 from the approach described in Section 3.3. Fig. 6 shows the evolution of the retrieved p-trigger and I-dose as well as a comparison between simulated and observed irrigations at district scale on a weekly basis. A good agreement is obtained with a bias, root mean square difference (RMSD) and correlation coefficient (R) between simulated and observed irrigation of − 0.038 hm^3, 0.154 hm^3 and 0.991, respectively. In fact, all observations fall within the estimated standard deviation of ensemble simulations.

Although the observed irrigations are well estimated by inverting both irrigation parameters (p-trigger and I-dose) simultaneously, I-dose is estimated with an overall high uncertainty: the temporal mean of the weekly temporal standard deviation is 4.1 mm. Such an uncertainty represents 45% of the temporal mean of retrieved I-dose (9.1 mm), and is even larger than the standard deviation (2.4 mm) evaluated in time

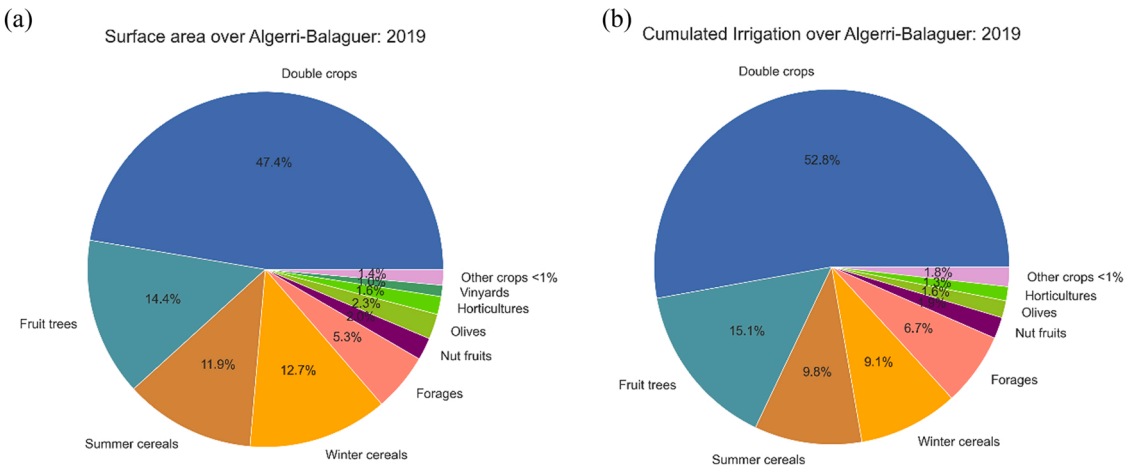

Fig. 5. Distribution of surface area (a) and estimated annual irrigation volume (b) by land cover class over Algerri-Balaguer irrigation district. Irrigation volumes are estimated for the year 2019 by running the classical FAO-2Kc over all crop fields in the district.

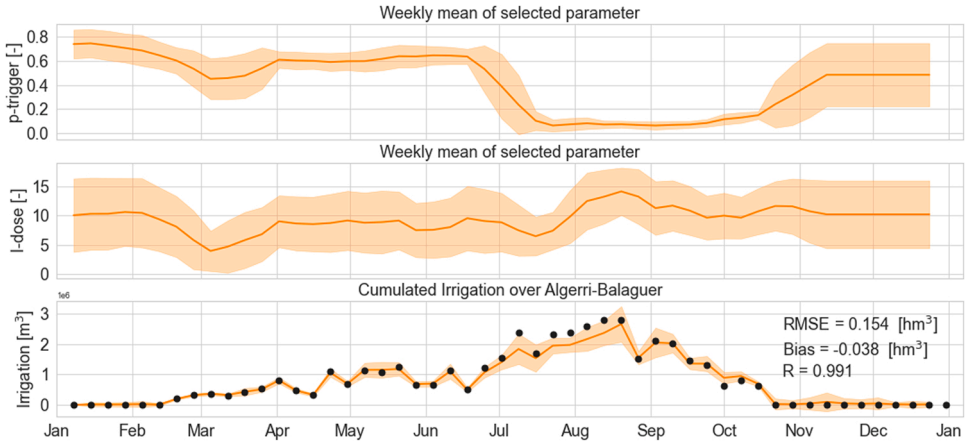

Fig. 6. Evolution of p-trigger and I-dose parameters estimated by assimilating irrigation observations during 2019. Shaded areas in three plots correspond to the standard deviation of parameter (line in the two top plots) and irrigation (line in the bottom plot) estimates. Observations are represented by circles in the bottom plot.

during 2019 of the weekly retrieved I-dose. In contrast, p-trigger is better retrieved with a much smaller relative uncertainty (25%). Moreover, the higher uncertainty in retrieved p-trigger during March is likely due to a compensation effect with the retrieved I-dose, whose uncertainty is reduced during the same period.

For the above reasons (insignificant temporal variations of retrieved I-dose, and possible compensation effects between retrieved p-trigger and I-dose), a choice is made to set the I-dose to a constant value, which is estimated as the mean of the weekly I-dose retrieved throughout the year. In practice, the assimilation approach is implemented a second time to retrieve p-trigger parameter in time (weekly scale) uniquely. In that case, I-dose is considered constant equal to 9 mm with an uncertainty of 4 mm, which are obtained from respectively the temporal mean of the retrieved I-dose and the temporal mean of the standard deviation at the weekly scale during 2019. Irrigation estimates from the assimilation approach using a fixed I-dose (Fig. 7) are even more accurate than using a time-varying I-dose with a bias, RMSD and R between simulated and observed irrigation of − 0.016, 0.084 hm^3 and 0.998, respectively.

As shown in Fig. 7, the time-varying p-trigger estimates show a progressive evolution representing the main two periods of irrigation throughout the year: from January to mid-June (until the end of spring) and from mid-July to September (summer). In the first period, p-trigger is well constrained with a small uncertainty lower than 0.1 and a slight decrease from 0.70 in January to 0.60 at mid-June, representing the gradual increase in irrigation water use in the district. According to the quite homogeneous SM_{WP} (0.207 m^3m^{-3}) and SM_{FC} (0.330 m^3m^{-3}) values in Algerri-Balaguer, the gradual increase in p-trigger represents a slight increase in $SM_{threshold}$ from 0.244 to 0.256 m^3m^{-3}. In contrast, the p-trigger retrieved during summer is very low with values ranging from 0.05 to 0.1 (depletion is always lower than 10% of TAW) and uncertainties around 0.04. The second irrigation period is thus characterized by an intense and frequent use of water, keeping the soil water content close to (or even above) SM_{FC}. Indeed, $SM_{threshold}$ is quite stable and close to SM_{FC} in summer with a value around 0.32 m^3m^{-3}. Between both periods (mid-June to early July), an abrupt change of p-trigger values is visible in Fig. 7. In fact, irrigation practices over the district completely change at that time, from a slight irrigation water use to an intense and frequent irrigation during summer. After summer (from October), irrigations are significantly diminished and thus the retrieved p-trigger increases. Note that the uncertainty in p-trigger is relatively large at that time because the FAO-2Kc stops the irrigation season when a decrease of 40% of maximum NDVI by field is detected. Consequently, when the irrigation season over annual crops is finished, there is not enough information to constraint p-trigger, which regains its original distribution (i.e., uniform distribution between 0.01 and 0.90).

In summary, p-trigger is accurately retrieved from irrigation observations by setting I-dose to a constant. Therefore, the estimated time-varying p-trigger and the constant I-dose fixed to 9 mm are used in

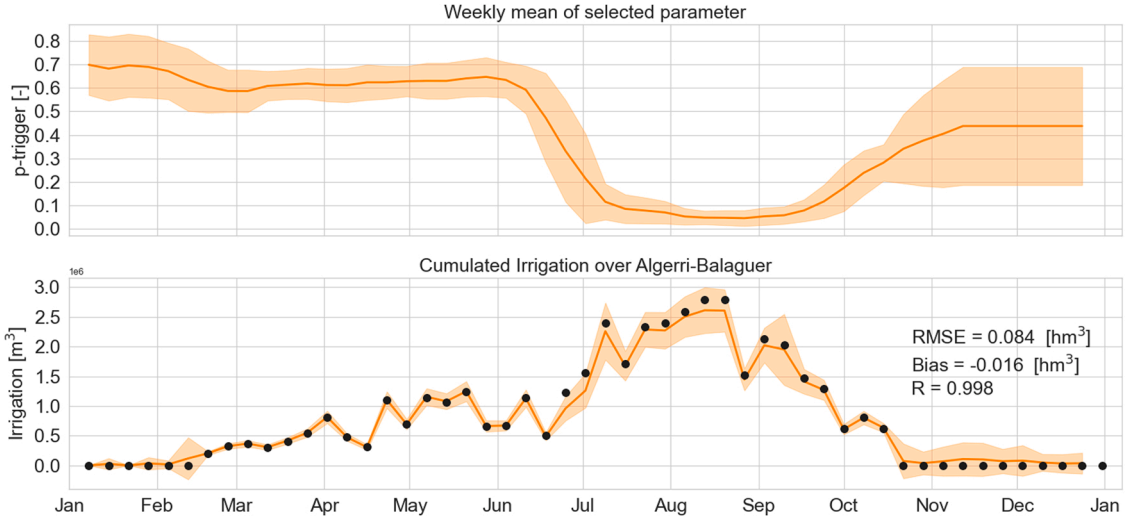

Fig. 7. Same as Fig. 6 but for the I-dose parameter set to a constant (the yearly mean of its weekly estimates).

our proposed approach (Var_Ret) to simulate irrigations over each crop field.

4.2. Comparing the four irrigation modules

The performance of the FAO-2Kc model using the Var_Ret irrigation module is evaluated for the five years (2017–2021) separately. To do so, the simulated irrigations from Var_Ret are compared against irrigation observations and results are also compared against those obtained using three different simplified configurations (Var_Fill, Fix_Fill, and Def_Fill) where $SM_{threshold}$ and I-dose are set to different values, as summarized in Table 2.

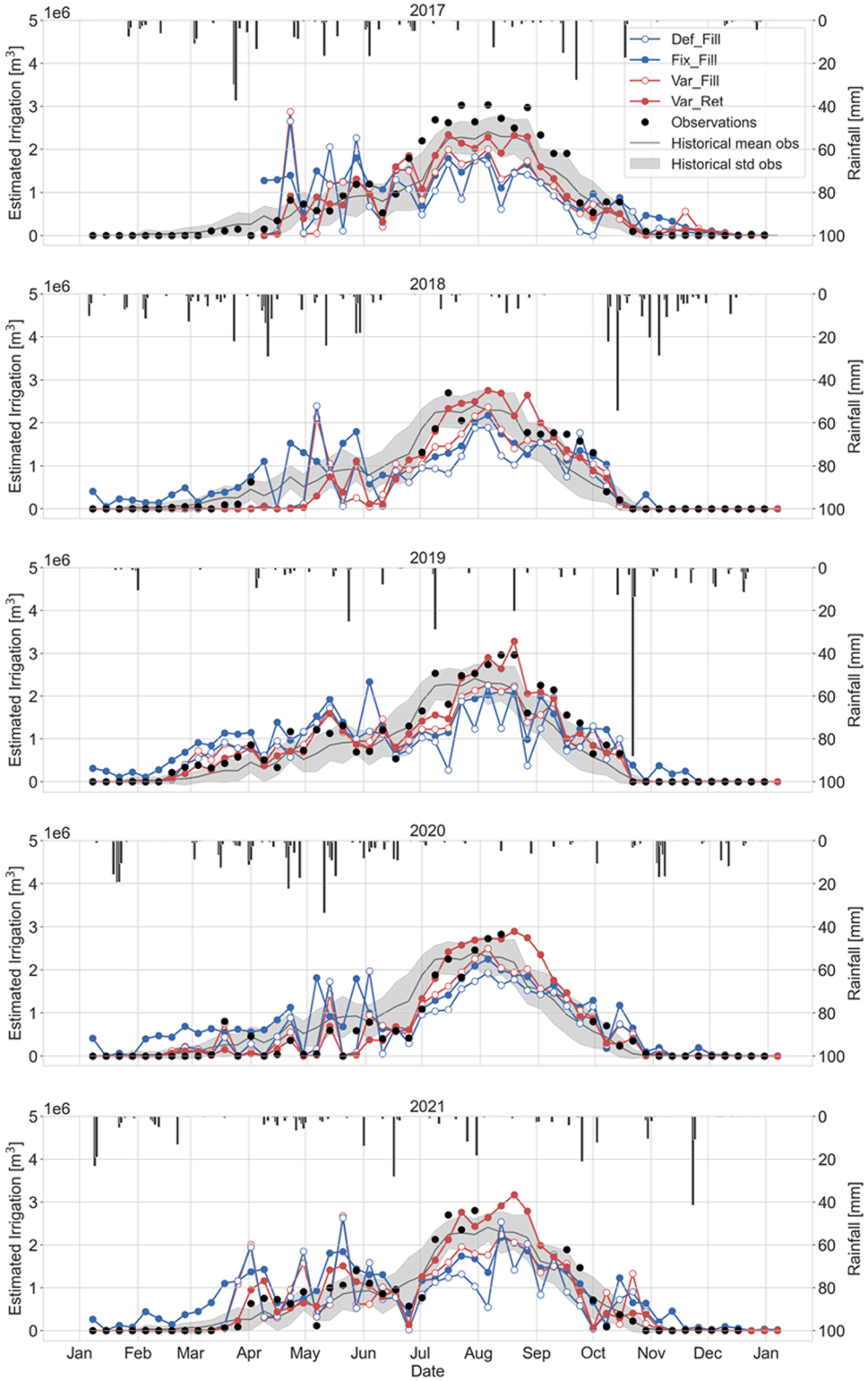

Fig. 8. Time series of irrigation estimates cumulated over Algerri-Balaguer district on a weekly basis for each year and from the four different irrigation modules separately: Def_Fill, Fix_Fill, Var_Fill and Var_Ret. Observed irrigations (black circles) as well as historical mean (from 2010 to 2022 period) and its standard deviation are also presented in gray line and shaded area, respectively.

The irrigation time series simulated by FAO-2Kc using the four irrigation modules are illustrated in Fig. 8 for each year separately. The historical mean and standard deviation of observed irrigations from 2010–2021 are also shown. In 2019 (the calibration year), Var_Ret is able to reproduce observed irrigations with a good precision throughout the year. For instance, the absence of irrigation from January to mid-February is well simulated. Similarly, the first irrigations in the district are adequately captured once the p-trigger threshold (0.78 in mid-February) is reached. From the beginning of the irrigation season until May, actual irrigations increase progressively, mainly because of the development of winter cereals covering about 60% of Algerri-Balaguer district (also represented in the double cropping class in Fig. 5). In June, irrigations slightly decrease due to changes from winter to summer cereals. At that time, senescent and initial stages of both agricultural seasons coexist in the district. In July and August, irrigations are very large mainly because of the development of maize – and its associated water requirement –, which covers about 60% of the surface area of the district (represented in summer cereals and double cropping classes in Fig. 5). In September, actual irrigations decrease once the senescent period of different crops (particularly maize) starts. This decrease is kept until the end of the irrigation season late October, from when the absence of irrigations is shown until the end of the year. All of the variations in irrigation water use described above are well represented by simulations from Var_Ret module.

In contrast, the other three irrigation modules are not capable to simulate adequately the dynamics of irrigations along the year. For instance, the absence of irrigations in January-February are not well represented by the modules that use a constant p-trigger (Def_Fill and Fix_Fill). Def_Fill simulates the first irrigations late January while Fix_Fill simulates them from the beginning of the year because a small water depletion (10% of TAW) is sufficient to trigger irrigations. Thus, Def_Fill and Fix_Fill simulate irrigations earlier since their fixed p-trigger values (~0.5 and 0.1, respectively) are smaller than the time-varying p-trigger used in Var_Ret in this period. Conversely, Var_Fill is able to reproduce the absence of irrigations in this period. In February-May period, the three modules that apply an irrigation dose to fulfill the soil water reservoir (Def_Fill, Fix_Fill and Var_Fill) overestimates irrigations with different dynamics between them given their different p-trigger values. In July-August period, these three modules are not capable to reproduce the high irrigation applied in the district, hence underestimating the actual irrigation amounts. At the end of the irrigation season, the three modules are roughly able to reproduce the decrease in irrigation water supply.

For the other years, the first actual irrigations start later than in 2019, i.e., from March to April. However, Var_Ret is still able to reproduce actual irrigations at the beginning of irrigation season for each year. As described above for the calibration year, the other three irrigation modules are not capable to estimate adequately the first irrigations of the year. While the Fix_Fill systematically overestimates irrigation from the beginning of the year, Def_Fill and Var_Fill are able to correctly simulate the absence of irrigation during the first months. However, Def_Fill and Var_Fill largely overestimate the first simulated irrigation because of important amounts of water are needed to fulfill the soil water storage after it was progressively depleted during the absence of irrigations, as it is clearly visible for 2017 and 2021. From the beginning of the irrigation season until May, with exception of 2020, actual irrigations increase to reach a peak related to the fully developed winter cereals. During the same period in 2020, weekly irrigations are much lower than for the other years varying between 0 (no-irrigation) and 0.8 hm^3. This is primarily because of large rainfall were observed in 2020, especially during April and May with a cumulated rainfall of 155 mm, which is much larger than the rainfalls observed in 2017, 2019 and 2021, i.e., 59, 60 and 45 mm, respectively. Similarly in 2018, Var_Ret simulates smaller irrigation amounts until May due to rainfall of 158 mm in April-May period. However, the agreement of simulations with observations in this period cannot be verified due to gaps in irrigation data. Nevertheless, it should be noted that Var_Ret is flexible enough to simulate accurately the irrigation water use during periods with completely different rainfall regimes than the one under which it was calibrated. Therefore, the proposed approach controlled by a time-varying threshold and a fixed I-dose that regulates irrigations allows to obtain estimations closer to the observations along the year. This is also valid when actual irrigations are very different among years.

During the summer months (particularly July and August), the Var_Ret configuration is capable to reproduce the large amounts of irrigation water use with an estimated RMSD of 0.48 (± 0.15) hm^3 and a bias of − 0.11 (± 0.34) hm^3. However, the configurations that fill the water reservoir are not as accurate with a RMSD ranging from 0.74 (± 0.27) to 1.16 (± 0.27) hm^3 and bias from − 0.62 (± 0.31) to − 1.05 (± 0.29) hm^3 for Var_Fill and Def_Fill modules, respectively. This means that an irrigation dose of 9 mm and a p-trigger value of 0.05 is suitable to reproduce the over-irrigation regime practiced in Algerri-Balaguer district during summer, unlike the other configurations that does not allow the FAO-2Kc model to over-irrigate. The latter is observed for all years, except for 2017 that present irrigation volumes very large from late June to mid-September, even above the historical mean plus a standard deviation. In turn, Var_Ret reproduces volumes similar to the historical irrigation amounts (2010–2021). Note that the larger irrigation observations during the summer 2017 are not attributable to any process represented by the FAO-2Kc as the development of crops, ET_0 and rainfall in summer are relatively similar for all the five years (2017–2021).

Fig. 9 illustrates the overall statistics of the comparison between simulated and observed irrigations for the four irrigation modules for each year separately. In the Taylor diagram, the standard deviation (STD) and centered-root mean square difference (RMSD) are normalized by the standard deviation of observations of each year separately. Such a normalization allows presenting the statistics of all years in a single graph and to be compared against a reference point representing a perfect simulation with R of 1, RMSD of 0 and normalized STD of 1 (i.e., the same as that of observations: 0.86 ± 0.12 hm^3). The diagram highlights the best performance obtained for the new approach (Var_Ret) with statistics systematically closer to the reference point for each year. For instance, Var_Ret systematically presents for all years the highest R of 0.95 (± 0.02), the lowest centered-RMSD of 0.27 (± 0.07) hm^3 and the STD closest to that of observations (0.81 ± 0.06 hm^3 equivalent to a normalized STD of 0.95 ± 0.12). On the right of Fig. 9, the bias in simulated irrigation is plotted against the RMSD. The best performance with a minimum bias is also systematically (for each year) obtained for Var_Ret. The new approach presents much better results than the classical irrigation modules, even in 2017 when all approaches significantly underestimate irrigations with a bias ranging between − 0.17 hm^3 and − 0.41 hm^3, and large RMSD between 0.45 and 0.96 hm^3. In addition to larger actual irrigation in 2017, this underestimation may be partially influenced by a lower irrigated area reported in the 2017 land cover map (8% less than the other years). With exception of 2017, the Var_Ret obtained a consistent RMSD around 0.24 (± 0.03) hm^3 and a bias around 0.02 (± 0.01) hm^3.

4.3. Discussions

The strategy of using a time-varying p-trigger and a fixed I-dose thus appears to be effective in improving the representation of irrigation practices along the year. Conversely, the classical approaches using fixed p-trigger and fulfilling the water storage capacity show the worst performances. In fact, Def_Fill and Fix_Fill modules present an overall R of 0.74 (± 0.14) and 0.79 (± 0.08), respectively, and RMSD of 0.62 (± 0.21) and 0.55 (± 0.14) hm^3, respectively. This classical irrigation scheme can be significantly improved when using a time-varying p-trigger and keeping the classical I-dose (Var_Fill), with an overall R of 0.86 (± 0.12) and RMSD of 0.45 (± 0.20) hm^3.

It should be noted that the irrigation regime is not known a priori. It

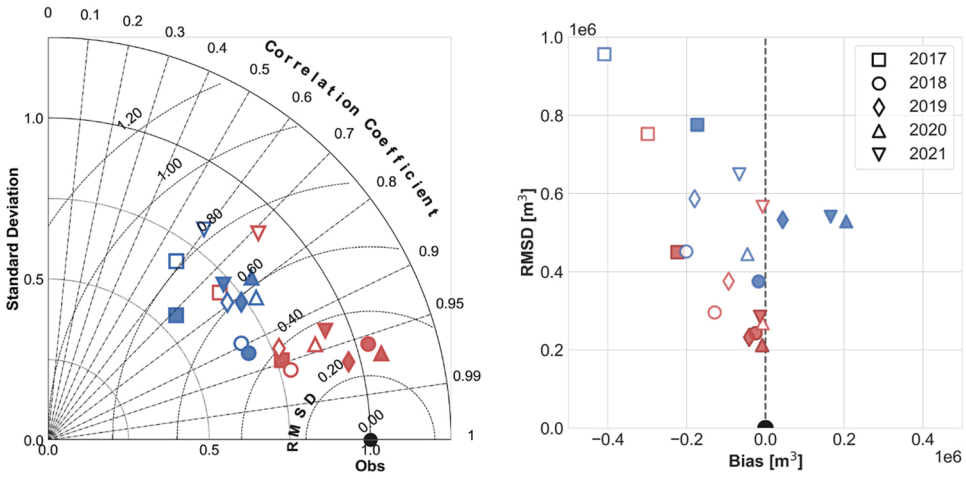

Fig. 9. Normalized Taylor diagram (on the left) and RMSD versus bias (on the right) summarizing statistics (correlation coefficient, R; normalized standard deviation, STD; and centered-root mean square difference, RMSD) between simulated and observed irrigation for each irrigation module (filled/empty blue/red symbols) and year (different symbols). In the Taylor diagram, normalized STD is on the radial axis, R is on the angular axis, centered-RMSD is the distance from a perfect simulation at the reference point (black filled circle) in the x-axis. The irrigation modules are represented as: Def_Fill (blue empty symbols), Fix_Fill (blue filled symbols), Var_Fill (red empty symbols), Var_Ret (red filled symbols).

is estimated from the difference between the observed irrigation and the optimal irrigation. The classical approach (Def_Fill) simulates the optimal irrigation that is the minimum water use (no water loss by deep percolation) that satisfies the crops requirement (no crop water stress). A deficit irrigation regime is hence evidenced by an observed irrigation lower than the optimal irrigation (generally in April-May) while an over-irrigation regime is evidenced by an observed irrigation larger than the optimal irrigation (systematically in July-August). Such a comparison between observed and optimal irrigation (Def_fill) is observed in Fig. 8. For example, in terms of annual irrigations in 2019 (the only year with no lack of data), the annual irrigation in optimal conditions (Def_Fill) is simulated at 35.4 hm^3 while actual irrigations is 44.8 hm^3. The over-irrigation is mainly concentrated during summer when actual irrigations in July-August amount to 21.3 hm^3 while the optimal volume satisfying the crops requirement during this period is estimated to 11.4 hm^3. Moreover, it is evidenced a deficit-irrigation regime in spring, when actual irrigation in April-May is 7.9 hm^3 while the optimal would be 9.4 hm^3. For the five years (2017–2021), the under-irrigation in April-May is estimated to -0.22 ± 0.07 hm^3/week while the over-irrigation in July-August is estimated to 1.05 ± 0.29 hm^3/week.

The Algerri-Balaguer irrigation district is thus under a deficit-irrigation regime in spring and an over-irrigation regime in summer. This can be explained by a misinterpretation of irrigation water needs by farmers who underestimate the water needs for winter cereals and overestimate them for maize, which are the main crops in the district covering about 60% of the total agricultural area. Therefore, considering a fixed p-trigger along the year is shown to be unreliable as it does not fit with the conception of local and traditional farmers. For instance, Var_Fill using a time-varying p-trigger provides a much better agreement with observations than using a fixed p-trigger as Def_Fill and Fix_Fill. However, the assumption of fulfilling the water reservoir may be unreliable for periods under important over-irrigation regimes. Therefore, the Def_Fill, Fix_Fill and Var_Fill modules are not suitable for irrigation district under deficit- and over-irrigation regimes.

Similar results to those obtained by Def_Fill and Fix_Fill, i.e. underestimating irrigation in summer and overestimating irrigation during the rest of the year, were also retrieved by Dari et al., (2020, 2022) from January 2016 to September 2017 over the same area (Algerri-Balaguer district) using a soil-moisture-based approach. The latter approach was proposed by Brocca et al. (2018) to estimate irrigation by inverting the water balance equation from the dynamics of coarse resolution satellite surface soil moisture products (e.g. SMAP, SMOS, ASCAT, AMSR-2). It has been evaluated using irrigation data at multiple scales and different satellite products (Dari et al., 2022, 2020; Jalilvand et al., 2019; Zhang et al., 2022). Dari et al. (2020) implemented two main improvements to estimate irrigation amounts at district scale: i) exploiting high-resolution (1 km) satellite soil moisture data and ii) adopting the FAO-2Kc ET formulation to adequately reproduce the crop ET over irrigated areas. They obtained a R of 0.76 over Algerri-Balaguer that is very close to that obtained in the present study for Def_Fill (0.74) and Fix_Fill (0.79). Then, Dari et al. (2022) evaluated the impact of different sources of ET in the same soil-moisture-based approach and found that the ET from the FAO-2Kc model showed the best performance.

Although ET process is critical in determining the soil water dynamics (Siebert and Döll, 2010), using reliable ET estimates at field scale is insufficient to invert irrigations accurately since different irrigation practices may lead to similar ET, especially in over-irrigation regime. Note that the parameters involved in the estimation of ET may vary according to the formulations of ET and of soil water transfers. Note however that the impact of physical parameters is limited in the case of over-irrigation, when the ET is controlled by the evaporative demand (and not by the soil water availability). To illustrate this point, Brombacher et al. (2022) recently proposed an irrigation retrieval approach based on the difference in remotely sensed ET between irrigated and natural (dry-land) vegetation cover. The authors implemented the method in the Ebro basin and evaluated the results on three plots close to the Algerri-Balaguer district. The retrieved monthly water use strongly underestimated the actual water use in Algerri-Balaguer.

A fixed I-dose is used for the Var_Ret module, consistent with the relatively large uncertainty in the monthly retrieved I-dose (see Fig. 5). Note that the I-dose is actually spatially and temporally variable due to diverse irrigation systems and practices within the area. The I-dose parameter is thus an effective value that represents the mean water amount applied per irrigation event over the district. Beyond the issue of non-representation of I-dose variabilities, the strength of the proposed approach is to represent with good accuracy the overall trend of irrigation practices (through the effective values of p-trigger and I-dose) at the scale of the irrigation district.

The PF assimilation method is thus a powerful tool that allows: i) taking into account the uncertainties of the model by means of input parameters errors, ii) incorporating prior information on the distribution of different variables, iii) estimating various parameters at the same time and iv) giving a realistic representation of the retrieved parameters and improving model's simulations. However, the major drawback is certainly the computational cost. Algorithms too computationally demanding can be impractical and even prohibitive for cases with a large data set. In this study however, we successfully reduced the computational cost by implementing the FAO56 model over the five main land covers only, instead of the ~3000 crop fields present in Algerri-Balaguer. This was possible because i) the five main crop types account for 94% of the total simulated irrigation over the district, ii) the area covered by each class is relatively uniform in terms of soil

properties and iii) vegetation states are also relatively uniform due to similar growing cycles per land cover class.

Another limitation of the proposed approach is the need for irrigation water use observations to calibrate $SM_{threshold}$ and I-dose, which are most often unavailable. In this study, we show that the irrigation module Var_Ret is capable of simulating irrigation accurately in all regimes (from deficit to excess irrigation). However, further studies should investigate alternative calibration approaches of the irrigation parameters without relying on in situ irrigation data. Especially, the assimilation of remotely sensed evapotranspiration soil moisture data could provide relevant information on irrigation practices (Kumar et al., 2015; Felfelani et al., 2018; Abolafia-Rosenzweig et al., 2019; Olivera-Guerra et al., 2020; Nie et al., 2022; Kwon et al., 2022). The increasing availability of high-resolution remote sensing data will foster the detection of irrigation events and of their impact on the actual crop water budget.

5. Conclusion

To date, the irrigation modules of land surface models have not yet been evaluated under different (e.g. deficit or excess) irrigation regimes, although agricultural practices greatly vary according to many (climatological, crop types, soil conditions, human, etc.) factors. Such irrigation modules are generally based on two parameters $SM_{threshold}$ and SM_{target} at which irrigation automatically starts and stops respectively, with an irrigation dose (I-dose) being a function of $SM_{threshold}$ and SM_{target}. In this study, we develop a new method to represent via $SM_{threshold}$ and I-dose the temporally varying irrigation water use of an irrigation district in any (optimal, deficit or even over) irrigation regime. To do that, we implement the FAO-56 dual crop coefficient (FAO-2Kc) model over the 8100 ha Algerri-Balaguer irrigation district and the temporal dynamics of the irrigation parameters ($SM_{threshold}$ and I-dose) are retrieved from the irrigation observations in 2019. Results are evaluated against irrigation observations over 5 years from 2017 to 2021. Based on this work, the following conclusions can be drawn:

- Inverting $SM_{threshold}$ variable at monthly scale with a fixed I-dose produces more accurate irrigation estimates than inverting both irrigation parameters ($SM_{threshold}$ and I-dose) at monthly scale.
- The seasonal evolution of the monthly retrieved $SM_{threshold}$ informs about the irrigation regime of both yearly irrigation periods in the district: a slight irrigation water use from winter to spring and an over-irrigation period during summer (with a $SM_{threshold}$ very close to SM_{FC}).
- The main difference between these two periods is due to a misinterpretation by farmers of the irrigation water needs of the main crops in the district (~60%). This results in a slight underestimation of the water needs for winter cereals (leading to a deficit irrigation regime) and a significant overestimation for maize (leading to an excess irrigation regime).
- The new irrigation scheme (Var_Ret) obtains systematically the best performance for each of the 5 years (2017–2021) compared to the other three tested modules with an overall R of 0.95 ($\pm$ 0.02) and a RMSD of 0.27 ($\pm$ 0.07) hm^3 (equivalent to a mean water depth over the district of 0.64 ± 0.17 mm/day). Especially, the monthly retrieved $SM_{threshold}$ improves significantly the performance of the classical FAO-56 irrigation module using a fixed $SM_{threshold}$ along the year. Moreover, setting I-dose to the amount needed to fill the root zone soil reservoir does not allow reproducing irrigation volumes under over-irrigation regimes, as occurring in summer in the Algerri-Balaguer district.
- Regardless of the variabilities of I-dose at the field scale due to diverse irrigation systems and practices, the strength of the proposed approach is to represent with good accuracy the overall trend of irrigation practices (through the effective values of $SM_{threshold}$ and I-dose) at the integrated scale of the irrigation district.

Given the strong consistency in terms of formalism and parameterization of the new irrigation module with existing modules based on $SM_{threshold}$ and SM_{target} parameters, the proposed approach can be implemented in a wide variety of land surface and hydrological models. Nevertheless, the calibration method of $SM_{threshold}$ and I-dose relies on irrigation water use measurements, which are rarely available worldwide. Another related issue is the assumption that the model parameters $SM_{threshold}$ and I-dose are uniform within the irrigation district, meaning that the same effective value is applied to different crop types and irrigation systems within the study area. In Algerri-Balaguer, maize largely dominates the water consumption of irrigation water in summer so that the variability of $SM_{threshold}$ is attributed to maize irrigation practices. However, irrigation practices may differ significantly over other areas with different crop types and irrigation systems, which would result in heterogeneous irrigation parameters within the district. Therefore, next studies should address both issues (requiring spatially distributed information on irrigation) by retrieving $SM_{threshold}$ and I-dose in both time and space. This could be achieved by assimilating remotely sensed evapotranspiration and soil moisture data (Abolafia-Rosenzweig et al., 2019; Felfelani et al., 2018; Kumar et al., 2015; Kwon et al., 2022; Nie et al., 2022). The use of remote sensing data related to irrigation will overcome the lack of in situ irrigation observations.

Declaration of Competing Interest

The authors declare that they have no known competing financial interests or personal relationships that could have appeared to influence the work reported in this paper.

Data Availability

Data will be made available on request.

Acknowledgements

This study was supported by the IDEWA project (ANR-19-P026-003) of the Partnership for research and innovation in the Mediterranean area (PRIMA) program and by the Horizon 2020 ACCWA project (grant agreement # 823965) in the context of Marie Sklodowska-Curie Research and Innovation Staff Exchange (RISE) program. The authors wish to acknowledge the "*Comunitat de Regants Canal Algerri Balaguer*" and the Ebro Hydrographic Confederation (SAIH Ebro) for providing the observation irrigation data used in this study.

References

Abolafia-Rosenzweig, R., Livneh, B., Small, E.E., Kumar, S.V., 2019. Soil moisture data assimilation to estimate irrigation water use. J. Adv. Model. Earth Syst. 11, 3670–3690. https://doi.org/10.1029/2019MS001797.

Allen, R.G., Pereira, L.S., Raes, D., Smith, M., 1998. Crop evapotranspiration: Guidelines for computing crop requirements. Irrig. Drain. Pap. No. 56, FAO 300. https://doi.org/10.1016/j.eja.2010.12.001.

Amazirh, A., Merlin, O., Er-Raki, S., Bouras, E., Chehbouni, A., 2021. Implementing a new texture-based soil evaporation reduction coefficient in the FAO dual crop coefficient method. Agric. Water Manag. 250, 106827 https://doi.org/10.1016/j.agwat.2021.106827.

AQUASTAT website, 2016. AQUASTAT - FAO's Information System on Water and Agriculture. Food Agric. Organ. United Nations.

Brocca, L., Tarpanelli, A., Filippucci, P., Dorigo, W., Zaussinger, F., Gruber, A., Fernández-Prieto, D., 2018. How much water is used for irrigation? A new approach exploiting coarse resolution satellite soil moisture products. Int. J. Appl. Earth Obs. Geoinf. 73, 752–766. https://doi.org/10.1016/j.jag.2018.08.023.

Brombacher, J., Silva, I.R., de, O., Degen, J., Pelgrum, H., 2022. A novel evapotranspiration based irrigation quantification method using the hydrological similar pixels algorithm. Agric. Water Manag. 267, 107602 https://doi.org/10.1016/j.agwat.2022.107602.

Chen, F., Mitchell, K., Schaake, J., Xue, Y., Pan, H.L., Koren, V., Duan, Q.Y., Ek, M., Betts, A., 1996. Modeling of land surface evaporation by four schemes and comparison with FIFE observations. J. Geophys. Res. Atmos. 101 https://doi.org/10.1029/95JD02165.

Dari, J., Brocca, L., Quintana-Seguí, P., Escorihuela, M.J., Stefan, V., Morbidelli, R., 2020. Exploiting high-resolution remote sensing soil moisture to estimate irrigation

water amounts over a mediterranean region. Remote Sens 12, 2593. https://doi.org/10.3390/rs12162593.
Dari, J., Quintana-Seguí, P., Morbidelli, R., Saltalippi, C., Flammini, A., Giugliarelli, E., Escorihuela, M.J., Stefan, V., Brocca, L., 2022. Irrigation estimates from space: Implementation of different approaches to model the evapotranspiration contribution within a soil-moisture-based inversion algorithm. Agric. Water Manag. 265, 107537 https://doi.org/10.1016/j.agwat.2022.107537.
Druel, A., Munier, S., Mucia, A., Albergel, C., Calvet, J.-C., 2022. Implementation and validation of a new irrigation scheme in the ISBA land surface model. Geosci. Model Dev. Discuss. 15, 8453–8471. https://doi.org/10.5194/gmd-15-8453-2022.
Felfelani, F., Pokhrel, Y., Guan, K., Lawrence, D.M., 2018. Utilizing SMAP soil moisture data to constrain irrigation in the community land model, 892-12,902 Geophys. Res. Lett. 45 (12). https://doi.org/10.1029/2018GL080870.
Foley, J.A., Ramankutty, N., Brauman, K.A., Cassidy, E.S., Gerber, J.S., Johnston, M., Mueller, N.D., O'Connell, C., Ray, D.K., West, P.C., Balzer, C., Bennett, E.M., Carpenter, S.R., Hill, J., Monfreda, C., Polasky, S., Rockström, J., Sheehan, J., Siebert, S., Tilman, D., Zaks, D.P.M., 2011. Solutions for a cultivated planet. Nature 478, 337–342. https://doi.org/10.1038/nature10452.
Foster, T., Mieno, T., Brozović, N., 2020. Satellite-based monitoring of irrigation water use: assessing measurement errors and their implications for agricultural water management policy. Water Resour. Res. 56 https://doi.org/10.1029/2020WR028378.
Fritsch, F.N., Carlson, R.E., 1980. Monotone piecewise cubic interpolation. SIAM J. Numer. Anal. 17, 238–246. https://doi.org/10.1137/0717021.
Gordon, N.J., Salmond, D.J., Smith, A.F.M., 1993. Novel approach to nonlinear/non-gaussian Bayesian state estimation. IEE Proceedings, Part F Radar Signal Process. 140. ⟨https://doi.org/10.1049/ip-f-2.1993.0015⟩.
Guimberteau, M., Laval, K., Perrier, A., Polcher, J., 2012. Global effect of irrigation and its impact on the onset of the Indian summer monsoon. Clim. Dyn. 39 https://doi.org/10.1007/s00382-011-1252-5.
Haddeland, I., Lettenmaier, D.P., Skaugen, T., 2006. Effects of irrigation on the water and energy balances of the Colorado and Mekong river basins. J. Hydrol. 324, 210–223. https://doi.org/10.1016/j.jhydrol.2005.09.028.
Hanasaki, N., Kanae, S., Oki, T., Masuda, K., Motoya, K., Shirakawa, N., Shen, Y., Tanaka, K., 2008. An integrated model for the assessment of global water resources - part 1: model description and input meteorological forcing. Hydrol. Earth Syst. Sci. 12. https://doi.org/10.5194/hess-12-1007-2008.
Hanasaki, N., Yoshikawa, S., Pokhrel, Y., Kanae, S., 2018. A global hydrological simulation to specify the sources of water used by humans. Hydrol. Earth Syst. Sci. 22, 789–817. https://doi.org/10.5194/hess-22-789-2018.
Hengl, T., De Jesus, J.M., Heuvelink, G.B.M., Gonzalez, M.R., Kilibarda, M., Blagotić, A., Shangguan, W., Wright, M.N., Geng, X., Bauer-Marschallinger, B., Guevara, M.A., Vargas, R., MacMillan, R.A., Batjes, N.H., Leenaars, J.G.B., Ribeiro, E., Wheeler, I., Mantel, S., Kempen, B., 2017. SoilGrids250m: global gridded soil information based on machine learning. PLoS One 12. https://doi.org/10.1371/journal.pone.0169748.
Jägermeyr, J., Gerten, D., Heinke, J., Schaphoff, S., Kummu, M., Lucht, W., 2015. Water savings potentials of irrigation systems: Global simulation of processes and linkages. Hydrol. Earth Syst. Sci. 19, 3073–3091. https://doi.org/10.5194/hess-19-3073-2015.
Jalilvand, E., Tajrishy, M., Ghazi Zadeh Hashemi, S.A., Brocca, L., 2019. Quantification of irrigation water using remote sensing of soil moisture in a semi-arid region. Remote Sens. Environ. 231, 111226 https://doi.org/10.1016/j.rse.2019.111226.
Krakauer, N.Y., Cook, B.I., Puma, M.J., 2020. Effect of irrigation on humid heat extremes. Environ. Res. Lett. 15. https://doi.org/10.1088/1748-9326/ab9ecf.
Kumar, S.V., Peters-Lidard, C.D., Santanello, J.A., Reichle, R.H., Draper, C.S., Koster, R. D., Nearing, G., Jasinski, M.F., 2015. Evaluating the utility of satellite soil moisture retrievals over irrigated areas and the ability of land data assimilation methods to correct for unmodeled processes. Hydrol. Earth Syst. Sci. 19, 4463–4478. https://doi.org/10.5194/hess-19-4463-2015.
Kwon, Y., Kumar, S.V., Navari, M., Mocko, D.M., Kemp, E.M., Wegiel, J.W., Geiger, J.V., Bindlish, R., 2022. Irrigation characterization improved by the direct use of SMAP soil moisture anomalies within a data assimilation system. Environ. Res. Lett. https://doi.org/10.1088/1748-9326/ac7f49.
Laluet, P., Olivera-Guerra, L., Rivalland, V., Simonneaux, V., Inglada, J., Bellvert, J., Er-Raki, S., Merlin, O., 2022. A sensitivity analysis of a Fao-56 dual crop coefficient-based model under various field conditions. Environ. Model 160, 105608. https://doi.org/10.1016/j.envsoft.2022.105608.
Lawrence, D.M., Fisher, R.A., Koven, C.D., Oleson, K.W., Swenson, S.C., Bonan, G., Collier, N., Ghimire, B., van Kampenhout, L., Kennedy, D., Kluzek, E., Lawrence, P.J., Li, F., Li, H., Lombardozzi, D., Riley, W.J., Sacks, W.J., Shi, M., Vertenstein, M., Wieder, W.R., Xu, C., Ali, A.A., Badger, A.M., Bisht, G., van den Broeke, M., Brunke, M.A., Burns, S.P., Buzan, J., Clark, M., Craig, A., Dahlin, K., Drewniak, B., Fisher, J.B., Flanner, M., Fox, A.M., Gentine, P., Hoffman, F., Keppel-Aleks, G., Knox, R., Kumar, S., Lenaerts, J., Leung, L.R., Lipscomb, W.H., Lu, Y., Pandey, A., Pelletier, J.D., Perket, J., Randerson, J.T., Ricciuto, D.M., Sanderson, B.M., Slater, A., Subin, Z.M., Tang, J., Thomas, R.Q., Val Martin, M., Zeng, X., 2019. The community land model version 5: description of new features, benchmarking, and impact of forcing uncertainty. J. Adv. Model. Earth Syst. 11, 4245–4287. https://doi.org/10.1029/2018MS001583.
Lehmann, P., Merlin, O., Gentine, P., Or, D., 2018. Soil texture effects on surface resistance to bare-soil evaporation, 398-10,405 Geophys. Res. Lett. 45 (10). https://doi.org/10.1029/2018GL078803.
Leng, G., Huang, M., Tang, Q., Sacks, W.J., Lei, H., Leung, L.R., 2013. Modeling the effects of irrigation on land surface fluxes and states over the conterminous United States: Sensitivity to input data and model parameters. J. Geophys. Res. Atmos. 118, 9789–9803. https://doi.org/10.1002/jgrd.50792.
Leng, G., Huang, M., Tang, Q., Gao, H., Leung, L.R., 2014. Modeling the effects of groundwater-fed irrigation on terrestrial hydrology over the conterminous United States. J. Hydrometeorol. 15, 957–972. https://doi.org/10.1175/JHM-D-13-049.1.
Leng, G., Huang, M., Tang, Q., Leung, L.R., 2015. A modeling study of irrigation effects on global surface water and groundwater resources under a changing climate. J. Adv. Model. Earth Syst. 7, 1285–1304. https://doi.org/10.1002/2015MS000437.
Massari, C., Modanesi, S., Dari, J., Gruber, A., De Lannoy, G.J.M., Girotto, M., Quintana-Seguí, P., Le Page, M., Jarlan, L., Zribi, M., Ouaadi, N., Vreugdenhil, M., Zappa, L., Dorigo, W., Wagner, W., Brombacher, J., Pelgrum, H., Jaquot, P., Freeman, V., Volden, E., Fernandez Prieto, D., Tarpanelli, A., Barbetta, S., Brocca, L., 2021. A review of irrigation information retrievals from space and their utility for users. Remote Sens. 13. https://doi.org/10.3390/rs13204112.
Merlin, O., Stefan, V.G., Amazirh, A., Chanzy, A., Ceschia, E., Tallec, T., Beringer, J., Gentine, P., Er-Raki, S., Bircher, S., Khabba, S., 2016. Modeling soil evaporation efficiency in a range of soil and atmospheric conditions: a downward approach based on multi-site data. Water Resour. Res. 52, 3663–3684. https://doi.org/10.1002/2015WR018233.
Milano, M., Ruelland, D., Dezetter, A., Fabre, J., Ardoin-Bardin, S., Servat, E., 2013. Modeling the current and future capacity of water resources to meet water demands in the Ebro basin. J. Hydrol. 500, 114–126. https://doi.org/10.1016/J.JHYDROL.2013.07.010.
Modanesi, S., Massari, C., Bechtold, M., Lievens, H., Tarpanelli, A., Brocca, L., Zappa, L., De Lannoy, G.J.M., 2022. Challenges and benefits of quantifying irrigation through the assimilation of Sentinel-1 backscatter observations into Noah-MP. Hydrol. Earth Syst. Sci. 1–31.
Moradkhani, H., Hsu, K.L., Gupta, H., Sorooshian, S., 2005. Uncertainty assessment of hydrologic model states and parameters: sequential data assimilation using the particle filter. Water Resour. Res. 41, 1–17. https://doi.org/10.1029/2004WR003604.
Nie, W., Kumar, S.V., Bindlish, R., Liu, P.-W., Wang, S., 2022. Remote sensing-based vegetation and soil moisture constraints reduce irrigation estimation uncertainty. Environ. Res. Lett. https://doi.org/10.1088/1748-9326/ac7ed8.
Oleson, K.W., Lawrence, D.M., Bonan, G.B., Drewniak, B., Huang, M., Koven, C.D., Levis, S., Li, F., Riley, W.J., Subin, Z.M., Swenson, S.C., Thornton, P.E., Bozbiyik, A., Fisher, R., Heald, C.L., Kluzek, E., Lamarque, J.-F., Lawrence, P.J., Leung, L.R., Lipscomb, W., Muszala, S., Ricciuto, D.M., Sacks, W., Sun, Y., Tang, J., Yang, Z.-L., 2013. Technical Description of version 4.5 of the Community Land Model (CLM).
Olivera-Guerra, L., Merlin, O., Er-Raki, S., 2020. Irrigation retrieval from Landsat optical/thermal data integrated into a crop water balance model: A case study over winter wheat fields in a semi-arid region. Remote Sens. Environ. 239 https://doi.org/10.1016/j.rse.2019.111627.
Ozdogan, M., Rodell, M., Beaudoing, H.K., Toll, D.L., 2010. Simulating the effects of irrigation over the united states in a land surface model based on satellite-derived agricultural data. J. Hydrometeorol. 11, 171–184. https://doi.org/10.1175/2009JHM1116.1.
Poggio, L., De Sousa, L.M., Batjes, N.H., Heuvelink, G.B.M., Kempen, B., Ribeiro, E., Rossiter, D., 2021. SoilGrids 2.0: producing soil information for the globe with quantified spatial uncertainty. SOIL 7. https://doi.org/10.5194/soil-7-217-2021.
Pokhrel, Y., Hanasaki, N., Koirala, S., Cho, J., Yeh, P.J.F., Kim, H., Kanae, S., Oki, T., 2012. Incorporating anthropogenic water regulation modules into a land surface model. J. Hydrometeorol. 13, 255–269. https://doi.org/10.1175/JHM-D-11-013.1.
Pokhrel, Y.N., Hanasaki, N., Wada, Y., Kim, H., 2016. Recent progresses in incorporating human land-water management into global land surface models toward their integration into Earth system models. Wiley Interdiscip. Rev. Water 3, 548–574. https://doi.org/10.1002/wat2.1150.
Puma, M.J., Cook, B.I., 2010. Effects of irrigation on global climate during the 20th century. J. Geophys. Res. Atmos. 115 https://doi.org/10.1029/2010JD014122.
Puy, A., Borgonovo, E., Lo Piano, S., Levin, S.A., Saltelli, A., 2021. Irrigated areas drive irrigation water withdrawals. Nat. Commun. 12. https://doi.org/10.1038/s41467-021-24508-8.
Román Dobarco, M., Cousin, I., Le Bas, C., Martin, M.P., 2019. Pedotransfer functions for predicting available water capacity in French soils, their applicability domain and associated uncertainty. Geoderma 336, 81–95. https://doi.org/10.1016/j.geoderma.2018.08.022.
de Rosnay, P., Polcher, J., Laval, K., Sabre, M., 2003. Integrated parameterization of irrigation in the land surface model ORCHIDEE. Validation over Indian Peninsula. Geophys. Res. Lett. 30 https://doi.org/10.1029/2003GL018024.
Scanlon, B.R., Keese, K.E., Flint, A.L., Flint, L.E., Gaye, C.B., Edmunds, W.M., Simmers, I., 2006. Global synthesis of groundwater recharge in semiarid and arid regions. Hydrol. Process. 20, 3335–3370. https://doi.org/10.1002/hyp.6335.
Scanlon, B.R., Faunt, C.C., Longuevergne, L., Reedy, R.C., Alley, W.M., McGuire, V.L., McMahon, P.B., 2012. Groundwater depletion and sustainability of irrigation in the US High Plains and Central Valley. Proc. Natl. Acad. Sci. U. S. A. 109, 9320–9325. ⟨https://doi.org/10.1073/pnas.1200311109⟩.
Shiklomanov, I.A., 2000. Appraisal and assessment of world water resources. Water Int. 25 https://doi.org/10.1080/02508060008686794.
Siebert, S., Döll, P., 2010. Quantifying blue and green virtual water contents in global crop production as well as potential production losses without irrigation. J. Hydrol. 384, 198–217. https://doi.org/10.1016/J.JHYDROL.2009.07.031.
Siebert, S., Burke, J., Faures, J.M., Frenken, K., Hoogeveen, J., Döll, P., Portmann, F.T., 2010. Groundwater use for irrigation - a global inventory. Hydrol. Earth Syst. Sci. 14, 1863–1880. https://doi.org/10.5194/hess-14-1863-2010.
Tang, Q., Oki, T., Kanae, S., Hu, H., 2007. The influence of precipitation variability and partial irrigation within grid cells on a hydrological simulation. J. Hydrometeorol. 8, 499–512. https://doi.org/10.1175/JHM589.1.

Thiery, W., Davin, E.L., Lawrence, D.M., Hirsch, A.L., Hauser, M., Seneviratne, S.I., 2017. Present-day irrigation mitigates heat extremes. J. Geophys. Res. 122, 1403–1422. https://doi.org/10.1002/2016JD025740.

Thiery, W., Visser, A.J., Fischer, E.M., Hauser, M., Hirsch, A.L., Lawrence, D.M., Lejeune, Q., Davin, E.L., Seneviratne, S.I., 2020. Warming of hot extremes alleviated by expanding irrigation. Nat. Commun. 11, 1–7. https://doi.org/10.1038/s41467-019-14075-4.

van Leeuwen, P.J., Künsch, H.R., Nerger, L., Potthast, R., Reich, S., 2019. Particle filters for high-dimensional geoscience applications: a review. Q. J. R. Meteorol. Soc. 145, 2335–2365. https://doi.org/10.1002/qj.3551.

Vrugt, J.A., ter Braak, C.J.F., Diks, C.G.H., Schoups, G., 2013. Hydrologic data assimilation using particle Markov chain Monte Carlo simulation: Theory, concepts and applications. Adv. Water Resour. 51, 457–478. https://doi.org/10.1016/J.ADVWATRES.2012.04.002.

Wada, Y., Van Beek, L.P.H., Bierkens, M.F.P., 2011. Modelling global water stress of the recent past: on the relative importance of trends in water demand and climate variability. Hydrol. Earth Syst. Sci. 15 https://doi.org/10.5194/hess-15-3785-2011.

Wada, Y., Wisser, D., Eisner, S., Flörke, M., Gerten, D., Haddeland, I., Hanasaki, N., Masaki, Y., Portmann, F.T., Stacke, T., Tessler, Z., Schewe, J., 2013. Multimodel projections and uncertainties of irrigation water demand under climate change. Geophys. Res. Lett. 40 https://doi.org/10.1002/grl.50686.

Wada, Y., Wisser, D., Bierkens, M.F.P., 2014. Global modeling of withdrawal, allocation and consumptive use of surface water and groundwater resources. Earth Syst. Dyn. 5, 15–40. https://doi.org/10.5194/esd-5-15-2014.

Zhang, K., Li, X., Zheng, D., Zhang, L., Zhu, G., 2022. Estimation of global irrigation water use by the integration of multiple satellite observations. Water Resour. Res 58. https://doi.org/10.1029/2021wr030031.